Research Article

Journal of RAMAN SPECTROSCOPY

Received: 16 November 2010 Accepted: 20 January 2011 Published online in Wiley Online Library: 31 March 2011

(wileyonlinelibrary.com) DOI 10.1002/jrs.2921

Dissection of dispersed off-resonant femtosecond degenerate four-wave mixing of O_2†

G. Knopp,* P. P. Radi, Y. Sych and T. Gerber

Simultaneous time and frequency detection in off-resonant femtosecond degenerate four-wave mixing (fs-DFWM) experiments displays spectral features that are covered in standard, nondispersed, frequency-integrated measurements. The application of laser fields with finite bandwidths, narrower than or comparable to the rotational Raman bands, affects the observed coherent signals. Information available from such experiments is split between the time and frequency domains and an improved measurement necessitates a combined detection. Rotational recurrences of oxygen (O_2), measured by dispersed fs-DFWM at room temperature, exhibit spectral characteristics, using 800-nm laser pulses with ∼100 fs duration. Analysis of the detected signals in both dimensions incorporating temporal and spectral trends can assist in the extraction and interpretation of chemicophysical quantities from the experiment. The dispersed recurrent signals are in accordance with simulations. Copyright © 2011 John Wiley & Sons, Ltd.

Keywords: time and frequency resolved; four-wave mixing; femtosecond; rotational recurrences

Introduction

Femtosecond (fs) four-wave mixing (FWM) spectroscopy has become an important tool for studying molecular dynamics in the gas phase.[1–9] The signals as a function of delay times between the applied laser pulses contain information on the coherences and the populations of quantum levels.[10] The detection at specific phase-matching geometries, as well as the time ordering of the applied laser pulses and their electric field polarization, selects the type of FWM process that is observed. Experiments have been carried out by using different techniques, e.g. coherent Stokes Raman scattering (CSRS) and coherent anti-Stokes Raman scattering (CARS),[7,11,12] degenerate four-wave mixing (DFWM), transient gratings[13] (TG), photon echo[14] (PE), polarization spectroscopy (PS)[2,15] and others.[16]

Because time-resolved FWM methods consist of the nonlinear interaction of three different, arbitrarily delayed light pulses, the signal generated in a medium depends on two delay times and four possible center frequencies (three-in, one-out) spanning a multidimensional variable space. For example, a time-resolved FWM experiment is performed by scanning the excitation frequencies and observing the dispersed spectrum of the signal pulse. For each delay time, a two-dimensional hypersurface of the multidimensional variable space is obtained. Such experiments are usually denoted as 'two-dimensional FWM spectroscopy'.[17–25] They provide the capability to establish correlations between quantum states within and between molecules if the number of experimentally controlled variables, such as frequencies of the interacting light or delay times between any two pulses, is larger than one.[24]

Dispersion of the signal field in combination with a variable time delay, e.g. yields the evolution of characteristic frequencies in the detected spectrum.[18,19,26] In electronically resonant fs-DFWM, different processes, such as CARS and CSRS, contribute at different wavelengths to the signal and contain valuable information on the specifically involved one-photon dipole transitions.[7] In contrast, the broadband excitation in electronically off-resonant fs-DFWM renders two-photon inelastic rotational Raman transitions possible and thus it is viewed as the time-domain analog of frequency-resolved coherent rotational Raman spectroscopy.

In standard off-resonance time-resolved FWM, two distinct density matrix time evolution pathways contribute to the signal. The two pump pulse interactions can either occur on the *bra* (pathway I) or on the *ket* (pathway II) side of the density matrix (Fig. 1). Pathway I finally produces a population change of Raman levels, whereas pathway II returns the system in its original population distribution. According to the excitation schemes, there are several ways how spectral components of pump and probe pulses can be arranged to produce a signal at a specific wavelength λ. Both initial Stokes (Fig. 1 left column) and anti-Stokes (Fig. 1 right column) transitions can contribute to red- and blue-shifted off-center wavelengths of the signal spectrum.[27] The probe pulse spectrum is modified accordingly for ultrashort probe pulses that exhibit a spectral width $\delta_{1/2}$ exceeding the Raman transitions $\tilde{\nu}_R$. A narrowed bandwidth of the probe laser pulse acts selectively on the process and dictates whether the optimal information from the measurement is achieved in the time-, frequency- or a combined detection domain.[19] For example, in 'hybrid' fs pump–ps probe vibrational CARS experiments, the application

* *Correspondence to: G. Knopp, General Energy Research Department, Paul Scherrer Institute, CH-5232 Villigen PSI, Switzerland. E-mail: gregor.knopp@psi.ch*

† *This article is part of the Journal of Raman Spectroscopy special issue entitled "Proceedings of the 9th European Conference on Nonlinear Optical Spectroscopy (ECONOS), Bremen, Germany, June 21–23, 2010" edited by Peter Radi (PSI, Villigen, Switzerland) and Arnulf Materny (JacobsUniversity, Bremen, Germany).*

General Energy Research Department, Paul Scherrer Institute, CH-5232 Villigen PSI, Switzerland

Journal of RAMAN SPECTROSCOPY

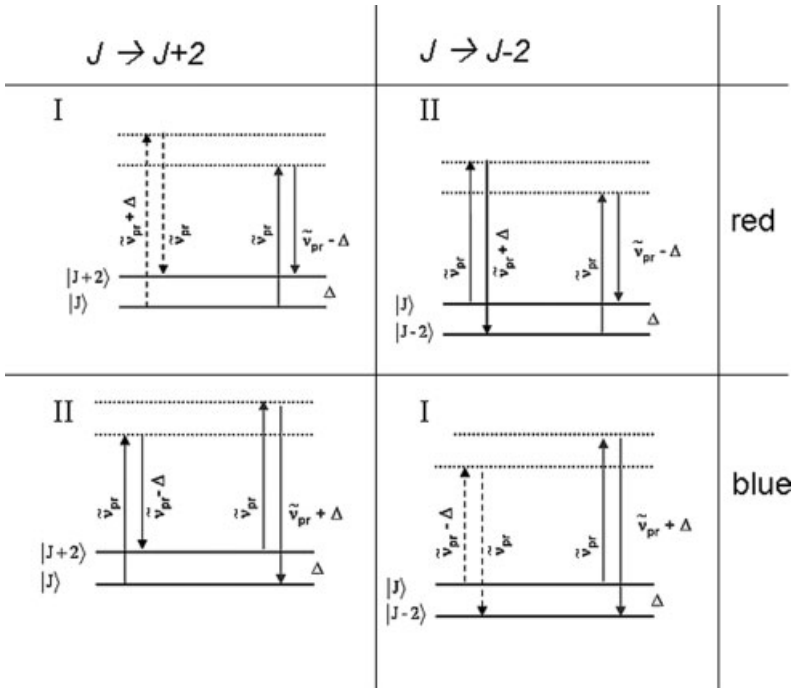

Figure 1. Specific wavelength contributions to the fs-DFWM signal spectrum. According to the excitation schemes, two distinct density matrix time evolution pathways (I + II) produce signal at Stokes (red) or anti-Stokes (blue) shifted wavelengths. In common notation, the dashed lines denote the *bra*- and straight lines the *ket*-side interactions on the density matrix.

of a narrowband probe generates signals from each involved Raman transition. The spectral width of the detected signals is determined either by the line width of the Raman transition or by the width of the probe, whichever is greater.[19]

In rotational electronically off-resonant fs-DFWM, the modulus squared of the polarization yields beating patterns that correspond to the sum and difference frequencies of individual Raman transitions. The spectrum of the signal is typically not considered, as it is believed that all information manifests in the evolution of the measured polarization as a function of time delay. However, if the finite bandwidth of the probe approaches the involved transitions, spectral changes start to become apparent. We observe that, using standard laser pulses of ~100 fs duration, the rotational recurrence signals from a gaseous O_2 sample, measured by dispersed fs-DFWM, significantly deviate from the probe pulse spectrum. The information available from the experiment is split between the time and frequency domains, and the combined detection displays spectrally distinct contributions at the observed revival times that are detuned from the central detection frequency.

Method

Time-resolved FWM methods imply the coherent interaction of three different light pulses with a medium to generate a signal pulse. In this paper, we confine ourselves to the off-resonance fs-DFWM technique with three parallel-polarized laser pulses crossing in a sample using a standard BOXCARS configuration. The angles are defined by placing apertures at the corners of a square and directing the beams along the main diagonals. The method is well known and therefore will be only briefly described.

Two beams arrive simultaneously at the sample and create a spatial interference pattern with a fringe spacing defined by the crossing angle and the wavelength of the incoming light. Molecular interaction with light at regions of high intensity induces a polarization that persists a long time after the initial light interaction. In fs-DFWM, the temporal evolution of this macroscopic polarization is governed by molecular rotations, orientation and population of Raman levels in the probe volume. A time-delayed (τ) probe pulse interrogates the induced polarization, and a signal field is generated that propagates in a phase-matched direction which is determined by the $\boldsymbol{k}$-vectors of the interacting fields: $\boldsymbol{k}_s = \boldsymbol{k}_1 - \boldsymbol{k}_2 + \boldsymbol{k}_3$.

In electronically off-resonance DFWM, it is convenient to express the third-order polarization $P^{(3)}$ by the two-photon Raman polarizabilities $\alpha_{ij}^{[l]}(\omega)$ of rank $l = 0, 1, 2$. For rotational Raman transitions in O_2 that contribute to the polarization, the induced anisotropy ($l = 2$) is of relevance and $\Delta J = \pm 2$ has to be fulfilled. The corresponding Raman shifts are $\hbar\omega_R = \hbar(\omega_i - \omega_j)$. The induced polarization can be described as[28]

$$P^{(3)}(t,\tau) \propto i \sum_{ij} p_{ij} \alpha_R^{[2]} \varepsilon_3(t) \exp[-i[(\omega_3 + \omega_R)t + \omega_R \tau]] + c.c. \quad (1)$$

where $\varepsilon_3(t) = \exp(-(a + ib)t^2)$ is the temporal Gaussian envelop of the applied probe laser field with $a = 2\ln(2)/t_{fwhm}^2$ and b accounting for a possible 'chirp'. For the off-resonant case, the transition amplitudes p_{ij} depend on the pump laser spectral shape and the population differences $\Delta\rho_{ij} = \rho_i - \rho_j$, with ρ_i denoting the population in state i[29]:

$$p_{ij} \propto \Delta\rho_{ij} \int_{-\infty}^{\infty} \varepsilon_1(\omega) \varepsilon_2^*(\omega - \omega_R) d\omega. \quad (2)$$

Hence, for stimulated Raman transitions to be excited by the pump pulses, the Raman frequencies must be within the spectral

bandwidth of the pulses. According to Eqns (1) and (2), the third-order polarization $P^{(3)}(t,\tau)$ appears as a Fourier transform of the transition amplitudes having a bandwidth that is determined by the convolution of the excitation pulses. A time-integrated homodyne detection method measures the absolute square of the induced polarization as function of the delay time.

$$S(\tau) = \int \mathrm{d}t \left|P^{(3)}(t,\tau)\right|^2 \tag{3}$$

Time-gated or dispersed detection methods measure either the temporal structure (variable t) or, equivalently, the spectrum of the polarization[30]:

$$S_{\mathrm{disp.}}(\omega,\tau) \propto \left|\int \mathrm{d}t\, P^{(3)}(t,\tau)\exp(-i\omega t)\right|^2 = \left|P^{(3)}(\omega,\tau)\right|^2 \tag{4}$$

In our experiments, the signal beam is dispersed in a monochromator and the spectral components are detected as function of the wavelength λ. A simulation of $S(\lambda,\tau) = 1/(2\pi c\omega^2)S(\omega,\tau)$ is given in Fig. 2 (top), in which the abscissa displays the delay and the ordinate depicts the spectrum of the signal. The intensity scales linearly from blue (low) to red (high) color.

With the rotational constant of oxygen $B_0 = 1.438\,\mathrm{cm}^{-1}$ and considering the zero nuclear spin of O_2 which allows only odd J quantum number states to be populated, the 'first' signal revival is observed at $\tau \sim (8B_0c)^{-1}$. The time between two full recurrences relates to the phase factors of the involved rotational wave functions when they advance by multiples of 2π (full rotations). The simulation confirms that rotational recurrences occur, the same as with integrated measurements,[2,16,31] with a periodicity of $\tau_{\mathrm{rec}} \sim 2.9$ ps. In a homodyne detection scheme, the fundamental rotational Raman transitions at $hc\,\tilde{\nu}_{\mathrm{R}} \cong \pm hc[(4B-6D)(J+3/2) - 8D(J+3/2)^3]$ with $\tilde{\nu}_{\mathrm{R}} = (2\pi\ c)^{-1}\ \omega_{\mathrm{R}}$ are not directly derived from a Fourier transform of the time-domain signals. Owing to the quadratic dependence on the polarization, the beating patterns in time-resolved off-resonant fs-DFWM correspond to absolute values of sums $|\tilde{\nu}_{\mathrm{R}} + \tilde{\nu}_{\mathrm{R}'}|$ and differences $|\tilde{\nu}_{\mathrm{R}} - \tilde{\nu}_{\mathrm{R}'}|$ of wavenumbers or Raman frequencies respectively, considering Stokes and anti-Stokes Raman transitions.

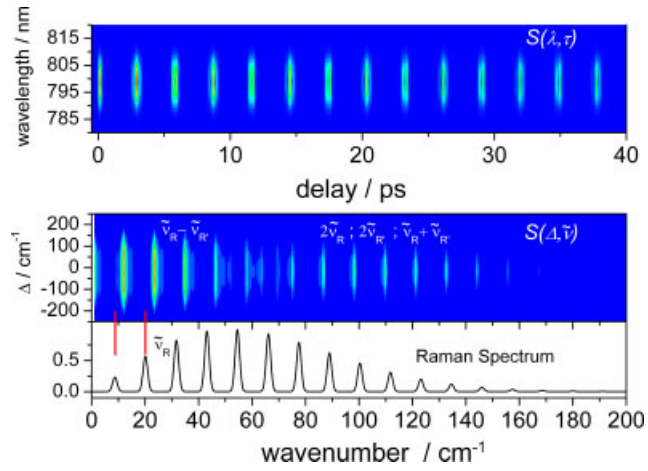

Figure 2. Top: Simulation of a dispersed fs-DFWM signal $S(\lambda,\tau)$ of O_2. Bottom: Beat wavenumbers derived by calculating the power spectral density in respect to the delay time τ. The ordinate displays the off-center wavenumber position $\Delta = \tilde{\nu} - \tilde{\nu}_0$ relative to the center wavenumber $\tilde{\nu}_0 = 1/\lambda_0$ [cm^{-1}] of the signal ($\Delta < 0$ red-shifted $\Delta > 0$ blue-shifted). The power spectrum contains the sum $|\tilde{\nu}_{\mathrm{R}} + \tilde{\nu}_{\mathrm{R}'}|$ and the difference $|\tilde{\nu}_{\mathrm{R}} - \tilde{\nu}_{\mathrm{R}'}|$ wavenumbers of Raman transitions $\tilde{\nu}_{\mathrm{R}}$. Comparison to a one-sided Raman spectrum calculation is given.

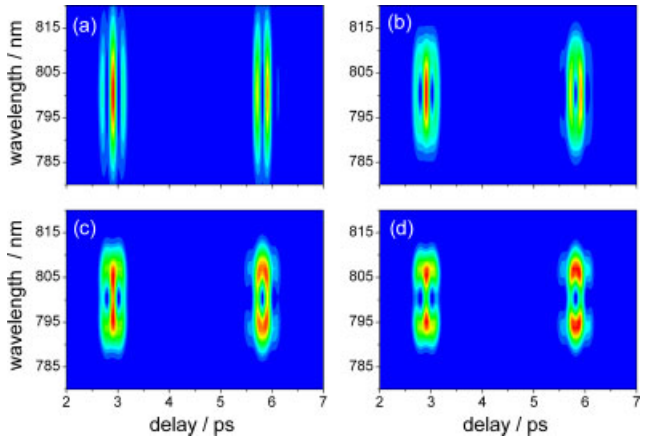

Figure 3. Simulation of dispersed broadband fs-DFWM signals of O_2 with 150 fs fwhm-ac (autocorrelation) pump-laser pulses and with 100/200/300/400 fs fwhm-ac (a)–(d) probe pulse widths. For short, thus spectrally broad probe pulses, all information is in the time domain (a), whereas considering probe pulses of longer duration and respectively narrower bandwidth, the information is split between the time and the frequency domain (b)–(d).

Figure 2 (bottom) depicts the power spectral densities of the simulated signal $S(\Delta,\tilde{\nu})$ at each spectral component. The detection wavelength λ has been transformed to wavenumber (energy) differences $\Delta = \tilde{\nu} - \tilde{\nu}_0$ [cm^{-1}] relative to the center probe photon wavenumber $\tilde{\nu}_0$ (= 12 500 cm^{-1} at λ_0 = 800 nm). The power spectrum of the simulation reflects two regions of peak positions. Significant intensity related to the difference frequency components is mainly observed at wavenumbers below ~80 cm^{-1}, while wavenumbers above ~80 cm^{-1} are attributed to sum frequency contributions or Stokes–anti-Stokes beating pairs. The first peak in the power spectrum occurs at 11.86 cm^{-1} corresponding to energy differences between neighboring O_2 Raman lines, the second peak relates to differences between the next but one Raman lines, and so forth. For comparison, a one-sided O_2 Raman spectrum calculation is depicted in Fig. 2 in which two transitions, corresponding to $\tilde{\nu}_{13}$ at 8.626 cm^{-1} and $\tilde{\nu}_{35}$ at 20.126 cm^{-1}, are indicated. The Raman band maximum is at ~55 cm^{-1}.

Zooming onto the first two recurrences, Fig. 3 depicts four dispersed fs-DFWM signal simulations with a fixed pump pulse duration of 150 fs fwhm-ac ('full width half maximum-autocorrelation') and for different probe pulse (assuming a Gaussian probe without chirp $b = 0$) durations of 100, 200, 300 and 400 fs fwhm-ac in the calculation. The simulation shows that for short, and therefore spectrally broad, probe pulses, all information is in the time domain (Fig. 3a), whereas considering probe pulses of longer duration and respectively narrower bandwidth, the information is split between the time and the frequency domain (Fig. 3b–d).

As generally expected, the spectral width of the observed reviving signal is reduced with increasing probe pulse duration (Fig. 3a and b). However, a further increase in the probe pulse duration (to 300 fs (fwhm-ac) Fig. 3c) does not significantly reduce the total spectral width of the dispersed revival. Instead, the signal splits and starts to maximize at wavenumbers that are detuned by approximately the sum wavenumber components. In this intermediate regime, the temporal information, however, is not yet completely blurred by the extended probe pulse duration.

Journal of RAMAN SPECTROSCOPY

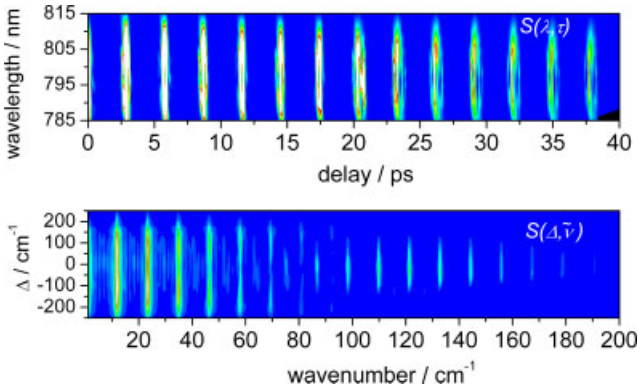

Figure 4. Dispersed broadband fs-DFWM signal of O_2. The observed rotational recurrences display spectral characteristics. The experimental and derived beat wavenumbers are in agreement with the simulations in Fig. 2.

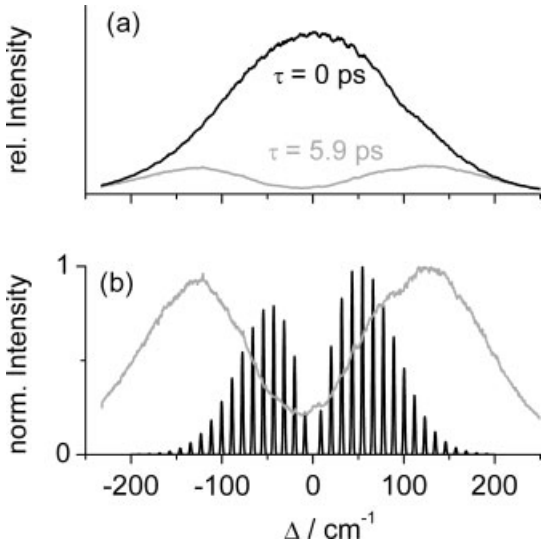

Figure 5. (a) Spectra measured at $\tau = 0$ and at $\tau = 5.9$ ps delay time. The nonresonant contribution at zero delay primarily reflects the spectrum of the probe. (b) At 5.9 ps delay, the spectrum of the signal has changed and shows a bimodal structure. The dispersed signal is compared to a Raman spectrum calculation including Stokes and anti-Stokes transitions.

Figure 3a and c (short and long probes) demonstrates that the detection close to the center wavelength $\lambda_0 = 800$ nm provides temporal information that is comparable to the interrogation with short probe pulses. However, the simulation shows that the center-wavenumber signal eventually approaches zero intensity if narrower bandwidth probe pulses are applied (Fig. 3d). In this case, the measurement transforms to a spectrally resolved experiment, with highest intensities at the frequency-shifted band maxima of the involved Raman transitions.

Experimental Setup

Fs-DFWM signals were spectrally resolved (Acton $f = 50$ cm, 1200 lines/mm) and detected by a charge coupled device (CCD) camera (1024 × 256 pixels, Princeton Instruments). The complete spectrum was measured at each time delay with a resolution of 0.46 cm^{-1}/pixel. Light pulses with pulse energies up to 20 μJ from a commercial fs-laser system (Clark-MXR CPA-1000) were used in the fs-DFWM experiments. The center wavelength of the laser emission is around 800 nm. The geometry of the BOXCARS arrangement was realized by placing a mask with four 5-mm diameter holes on a square of 25 mm lateral length in front of a $f = 500$ mm lens focusing the incoming laser beams to one spot. Typical properties of the near-infrared light pulses, characterized with a compact second-harmonic FROG (frequency-resolved optical gating) system (Grenouille UPM-8-20 with Video FROG software), are ∼100 fs (fwhm) pulse width (∼155 fs fwhm-ac), a spectral bandwidth of ∼11 nm and a time–bandwidth product of ∼0.52.

Results and Discussion

Dispersed fs-DFWM from a 100-mbar O_2 sample was measured. The result is displayed in Fig. 4 for delay times up to 40 ps. Comparison with the simulation of Fig. 2 confirms the correct modeling of $S(\lambda, \tau)$ and $S(\Delta, \tilde{\nu})$ by observing the expected sum and difference wavenumbers in the power spectral density. According to Fig. 4, essential intensity contributions can be observed at off-center wavenumbers. While the sum frequency components of $S(\Delta, \tilde{\nu})$ are at maximum intensity at the center line $\Delta = 0\ cm^{-1}$, the difference frequency components have their highest intensity at off-center detection. At $\Delta \geq \pm 120\ cm^{-1}$, the sum frequency components are missing in the power spectrum, indicating that far separated Stokes–anti-Stokes beating pairs are absent, whereas increased intensity in the difference frequency components is observed at these spectral positions.

Figure 5a compares the spectra measured at $\tau = 0$ and at $\tau = 5.9$ ps delay time. The nonresonant contribution at zero delay is the product of the pump electric fields and the signal spectrum, primarily reflecting the spectrum of the probe. At 5.9 ps delay, the signal spectrum has changed and depicts a bimodal structure. A comparison to a Raman spectrum calculation, including Stokes and anti-Stokes transitions, is made in Fig. 5b.

Figure 6a displays the first two recurrences $[S(\lambda, \tau)]$ of O_2 in more detail. Due to their appearance in the two-dimensional presentation, we refer to them as ϕ- and O-shaped revivals. The ϕ-shaped form corresponds to quarter or three-quarter revivals, whereas the O-shapes relate to half or full revivals. The experiment presented in Fig. 6a is consistent with the simulations in Fig. 3, considering a probe pulse width between 200 and 300 fs (fwhm-ac). With the assumption of transform-limited Gaussian light pulses, this corresponds to our typical experimental conditions. The calculated O- and ϕ-type spectral characteristics are well observed in the dispersed measurement. In a perfect time-resolved fs-DFWM experiment, all excited molecules recapture their initial orientation at exact full revival times. Therefore, starting with an isotropic sample yields isotropy again at the full revival times and no phase-matched signal is expected to emerge at these delays. For homonuclear diatomic molecules, the polarizability parallel ($\alpha_{||}$) to the molecular axis is more efficient than that perpendicular to it ($\alpha_{\perp}$) and the effective refraction index is increased for field polarizations that are oriented parallel to the molecular axis and decreased for a perpendicular orientation.

At the 5.8-ps O-shaped half revival time, the probed molecules rotate from a perpendicular to a parallel orientation relative to the electrical field vector of the laser pulses. As a consequence, the induced refractive index decreases just before and increases right after the exact revival time. However, due to the modulus squared of the polarization, fs-DFWM is only sensitive to the amplitude of the refraction index change and not to its sign. At 2.9 ps, the main

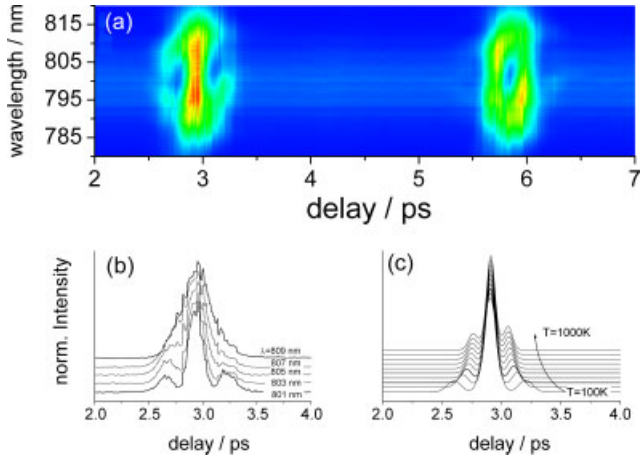

Figure 6. (a) Dispersed fs-DFWM measurement of the first ϕ- and O-shaped quarter (at ~2.9 ps) and a half revival (at ~5.8 ps) of O_2. (b) Sections of the quarter revival at five detection wavelengths. (c) Simulation of the temperature dependence of the integrated signal for temperatures from 100 to 1000 K.

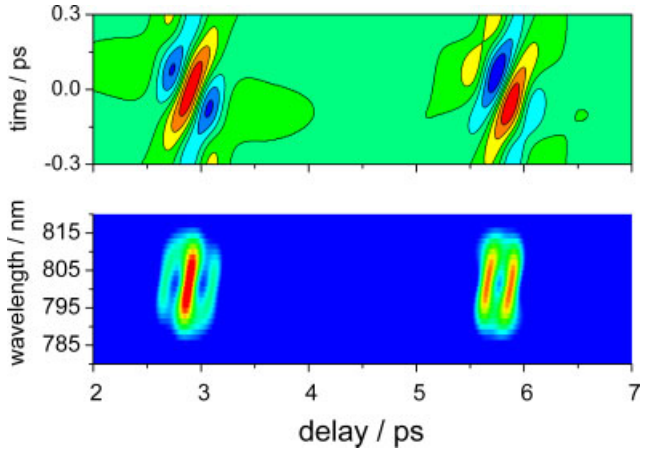

Figure 7. Top: $n(t, \tau)$: Change of the refractive index as a function of time and the time delay. Red color denotes an increase, while the blue indicates a decrease from the average n_0 (green). Bottom: Simulation of a dispersed broadband fs-DFWM signal of O_2. The probe pulse is chirped to reproduce the skewness of the signal in the experiment.

peak of the ϕ-type quarter revival is due to an increase in refractive index, whereas the two side peaks result from a decreased refractive index. In an integrated one-dimensional experiment, this leads to the triple peak signal characteristic of the quarter revival. Elongated probe pulse durations confine the temporal resolution in the experiment and mask the double or triple peaked signal progression. In the dispersed two-dimensional measurement, however, it becomes evident that smearing of the signal mainly occurs at off-center frequencies, resulting in the observed O- and ϕ-shaped structures. Close to λ_0, the temporal structure of the signal is rather well preserved. Figure 6b displays cuts of the ϕ-type revival at five different spectral positions from 801 to 809 nm. Towards larger off-center detection, the revival structure blurs, and finally at wavelength >809 nm ($\Delta > 123$ cm^{-1}) it displays only a singly peaked structure. The width and position of the side peaks are important for the accurate determination of temperatures or spectroscopic constants from the integrated measurements. The effect of the temperature is that it shifts the population of the initial state distribution towards higher J quantum numbers, yielding narrowed peak widths and a larger separation the double and triple peak structures with increasing temperature. The simulations in Fig. 6c show the change of the quarter revival with temperature in nondispersed fs-DFWM, assuming a 200-fs fwhm-ac probe pulse. Comparison with Fig. 6b shows that the detection wavelength dependence on the signal differs from the calculated temperature dependence. However, both effects affect the appearance and position of the side peaks, and a consequent temperature derivation may be blurred.

Interestingly, in a somehow counterintuitive way, the temporal resolution of the experiment is still preserved in the center of the spectrum within a spectral window that is smaller than the spectrum of the nonresonant contribution (Fig. 5b). Within this limited spectral range, a clear temporal structure of the revivals is still observed due to the persistence of the sum frequency components.

On closer inspection, it can be seen that the O- and ϕ-shaped structures in Fig. 6a are skewed. In our opinion, this skewness is caused by the slight phase distortions of the probe pulse. By considering only quadratic phase distortions of the probe pulse $\phi_t = -bt^2$ ($b \neq 0$), an analytic expression of Eqn (4) is deducible and the Fourier transformed polarization becomes (see Appendix)

$$P^{(3)}(\varpi, \tau) \propto i \sum_{\mathrm{R}} p_{\mathrm{R}} \alpha_{\mathrm{R}}^{[2]} \varepsilon_3(\varpi) \exp\left[-i\left[\frac{\tau_{\mathrm{g}}}{2}\varpi + \omega_{\mathrm{R}}\tau\right]\right] + c.c. \quad (5)$$

with $\varpi = \omega - \omega_3 - \omega_{\mathrm{R}}$ and a group delay $\tau_{\mathrm{g}} = \dfrac{b}{2(a^2+b^2)}\varpi$, which is linearly proportional to the frequency. A linear phase shift in time does not affect the instantaneous frequency and leads to a constant group delay. However, it is the effect of the frequency-dependent group delay that induces an asymmetric response in the time–frequency plane. For elucidation, the fs-DFWM signal can be considered as probe pulse refraction, due to an induced deviation of the average refractive index in the probe volume. For small deviations, the time-dependent change of the refractive index $\Delta n(t, \tau) = n(t, \tau) - n_0$ is in essence linearly proportional to the induced third-order polarization.[32]

$$\Delta n(t, \tau) \approx \frac{P^{(3)}(t, \tau)}{2\varepsilon_0 n_0 E_3(t)} \quad (6)$$

A simulation of the refractive index as function of t and τ is plotted in Fig. 7. Red color denotes the increase, while blue indicates the decrease from the average n_0 (green). Changes due to molecular rotation appear whenever $\tau - t$ (with $t = 0$ as center of the probe) corresponds to full-, half,- or any partial revival time T_{rev}. If the frequency of the probe pulse changes with time t, the asymmetry or dispersion $n(t, \tau) \rightarrow n(\omega, \tau)$ of the refractive index during the probing time yields to an asymmetry of the observed signal spectrum in dispersed fs-DFWM. The simulation in Fig. 6 (bottom) reflects the observed asymmetry of the measurement (Fig. 6a) by incorporating a second-order phase distortion with $b \cong 0.3a$. Higher order terms have not been considered. From this perspective, the dispersed DFWM method allows an '*in situ*' pulse characterization of the probe pulse during the measurement, as it basically resembles a FROG analysis. A detailed analysis of the molecular response as a function of specific phase distortions is beyond the scope of this paper.

Conclusions

Dispersed fs-DFWM signals of O_2 were measured and simulated. The application of spectral pulse widths that are in the order of the Raman transitions transfers the measurement to an intermediate regime in which the information extractable from the signals is split between the time and frequency domains. These conditions are readily met for frequently used experimental conditions. While the pump pulse excitation merely affects the relative amplitudes of the involved rotational contributions, spectral positions and line shapes are primarily determined by the finite bandwidth of the probe pulse. Disregarding the benefit of an increased spectral selectivity, the temporal structure of the transient signal becomes indistinct by the application of a rather narrowband probe pulse in a one-dimensional measurement. In contrast, the broadband preparation in combination with the frequency-resolved multichannel acquisition partially enables a separation of the frequency components of the induced polarization. A two-dimensional time–frequency analysis of the dispersed recurring signals of O_2, e.g. reveals an increase of signal strength at spectral positions off the center wavelength of the probe. A Fourier analysis at these spectral positions mainly yields the Raman difference frequency components, while the sum frequency contributions have disappeared. Close to the center detection wavelength, however, no significant blurring of the transient signal was found and the fastest temporal features corresponding to Raman sum frequencies contribute to the time response of the experiment. Viewing the time–frequency plane, the quarter- and half-revivals of O_2 display ϕ- and O-shaped forms in agreement with the simulation, and the time evolution of the signal observed considerably depends on the detection wavelength.

Appendix

Referring to Eqn (1), the time and delay time-dependent third-order polarization is

$$P^{(3)}(t,\tau) \propto i \sum_{\mathrm{R}} p_{\mathrm{R}} \alpha_{\mathrm{R}} \varepsilon_3(t) \exp\left[-i\left[(\omega_3+\omega_{\mathrm{R}})t+\omega_{\mathrm{R}}\tau\right]\right] + c.c. \quad \text{(A1)}$$

Considering a Gaussian probe pulse envelope and a quadratic phase distortion b

$$\varepsilon_3(t) = \varepsilon_t \exp[-at^2] \exp[-i(bt^2)] \quad \text{(A2)}$$

the polarization becomes

$$P^{(3)}(t,\tau) \propto i \sum_{\mathrm{R}} p_{\mathrm{R}} \alpha_{\mathrm{R}} \varepsilon_t \exp\left[-at^2\right] \exp[-i((\omega_3+\omega_{\mathrm{R}})t+bt^2)] \exp\left[-i\omega_{\mathrm{R}}\tau\right]. \quad \text{(A3)}$$

Fourier transformation yields the polarization as a function of frequency and delay time:

$$P^{(3)}(\omega,\tau) = F\{P^{(3)}(t,\tau)\} \quad \text{(A4)}$$

The Fourier transformation of a linearly chirped Gaussian pulse $E(t) = E_t \exp[-at^2] \exp[-i(\omega_0 t + bt^2)]$ is

$$F\{E(t)\} = E(\omega) = E_\omega \exp\left[-\frac{1}{4(a-ib)}(\omega-\omega_0)^2\right] = E_\omega \exp\left[-\frac{a}{4(a^2+b^2)}(\omega-\omega_0)^2\right] \exp\left[-i\frac{b}{4(a^2+b^2)}(\omega-\omega_0)^2\right] \quad \text{(A5)}$$

The Fourier-transformed polarization becomes

$$P^{(3)}(\omega,\tau) \propto i \sum_{\mathrm{R}} p_{\mathrm{R}} \alpha_{\mathrm{R}} \varepsilon_\omega \exp\left[-i\omega_{\mathrm{R}}\tau\right] \exp\left[-\frac{(\omega-\omega_3-\omega_{\mathrm{R}})^2}{4a}\right] \exp\left[-\frac{ib(\omega-\omega_3-\omega_{\mathrm{R}})}{2(a^2+b^2)}\right] \quad \text{(A6)}$$

With $\varpi = \omega - \omega_3 - \omega_{\mathrm{R}}$ and $\tau_{\mathrm{g}} = \frac{b}{2(a^2+b^2)}\varpi$, we derive the expression of Eqn (5):

$$P^{(3)}(\varpi,\tau) \propto i \sum_{\mathrm{R}} p_{\mathrm{R}} \alpha_{\mathrm{R}} \varepsilon_3(\varpi) \exp\left[-i\left[\frac{\tau_{\mathrm{g}}}{2}\varpi + \omega_{\mathrm{R}}\tau\right]\right] \quad \text{(A7)}$$

References

[1] M. Dantus, V. V. Lozovoy, *Chem. Rev.* **2004**, *104*, 1813.
[2] H. M. Frey, P. Beaud, T. Gerber, B. Mischler, P. P. Radi, A. P. Tzannis, *Appl. Phys. B-Lasers Opt.* **1999**, *B68*, 735.
[3] G. Knopp, I. Pinkas, Y. Prior, *J. Raman Spectrosc.* **2000**, *31*, 51.
[4] G. Knopp, P. Radi, M. Tulej, T. Gerber, P. Beaud, *J. Chem. Phys.* **2003**, *118*, 8223.
[5] T. Lang, M. Motzkus, H. M. Frey, P. Beaud, *J. Chem. Phys.* **2001**, *115*, 5418.
[6] M. Motzkus, S. Pedersen, A. H. Zewail, *J. Phys. Chem.* **1996**, *100*, 5620.
[7] M. Schmitt, G. Knopp, A. Materny, W. Kiefer, *Chem. Phys. Lett.* **1997**, *280*, 339.
[8] A. M. Walser, P. Beaud, P. P. Radi, M. Tulej, T. Gerber, G. Knopp, *J. Raman Spectrosc.* **2007**, *38*, 147.
[9] A. M. Walser, M. Meisinger, P. P. Radi, T. Gerber, G. Knopp, *Phys. Chem. Chem. Phys.* **2009**, *11*, 8456.
[10] S. Mukamel, *Principles of Nonlinear Optical Spectroscopy*, Oxford University Press: New York, **1995**.
[11] M. Schmitt, G. Knopp, A. Materny, W. Kiefer, *Chem. Phys. Lett.* **1997**, *270*, 9.
[12] I. Pinkas, G. Knopp, Y. Prior, *J. Chem. Phys.* **2001**, *115*, 236.
[13] E. J. Brown, Q. G. Zhang, M. Dantus, *J. Chem. Phys.* **1999**, *110*, 5772.
[14] M. Comstock, V. V. Lozovoy, M. Dantus, *J. Chem. Phys.* **2003**, *119*, 6546.
[15] V. V. Matylitsky, W. Jarzeba, C. Riehn, B. Brutschy, *J. Raman Spectrosc.* **2002**, *33*, 877.
[16] M. Dantus, I. Pastirk, V. V. Lozovoy, B. I. Grimberg, *Abstr. Papers Am. Chem. Soc.* **2000**, *220*, U241.
[17] K. A. Meyer, J. C. Wright, D. E. Thompson, *J. Phys. Chem. A* **2004**, *108*, 11485.
[18] A. V. Pakoullev, M. A. Rickard, K. A. Meyer, K. Kornau, N. A. Mathew, D. E. Thompson, J. C. Wright, *J. Phys. Chem. A* **2006**, *110*, 3352.
[19] D. Pestov, R. K. Murawski, G. O. Ariunbold, X. Wang, M. C. Zhi, A. V. Sokolov, V. A. Sautenkov, Y. V. Rostovtsev, A. Dogariu, Y. Huang, M. O. Scully, *Science* **2007**, *316*, 265.
[20] L. R. Valachovic, M. F. Tuchler, M. Dulligan, T. D. Georget, M. Zyrianov, A. Kolessov, H. Reisler, C. Wittig, *J. Chem. Phys.* **2000**, *112*, 2752.
[21] M. H. Cho, *Chem. Rev.* **2008**, *108*, 1331.
[22] M. H. Cho, T. Brixner, I. Stiopkin, H. Vaswani, G. R. Fleming, *J. Chin. Chem. Soc.* **2006**, *53*, 15.
[23] S. Hahn, K. Kwak, M. Cho, *J. Chem. Phys.* **2000**, *112*, 4553.
[24] D. M. Jonas, *Annu. Rev. Phys. Chem.* **2003**, *54*, 425.
[25] S. Mukamel, *Annu. Rev. Phys. Chem.* **2000**, *51*, 691.
[26] R. P. Lucht, *Science* **2007**, *316*, 207.
[27] L. D. Ziegler, R. Fan, A. E. Desrosiers, N. F. Scherer, *J. Chem. Phys.* **1994**, *100*, 1823.
[28] A. Shalit, Y. Paskover, Y. Prior, *Chem. Phys. Lett.* **2008**, *450*, 408.
[29] D. Meshulach, Y. Silberberg, *Phys. Rev. A* **1999**, *60*, 1287.
[30] R. Zadoyan, D. Kohen, D. A. Lidar, V. A. Apkarian, *Chem. Phys.* **2001**, *266*, 323.
[31] V. G. Stavros, E. Harel, S. R. Leone, *J. Chem. Phys.* **2005**, *122*.
[32] R. W. Boyd, *Nonlinear Optics* (2nd edn), Academic Press: Amsterdam, **2003**.